November 4th 2016

Horizontally acquired AT-rich genes in *Escherichia coli* cause toxicity by sequestering RNA polymerase

Lisa E. Lamberte[1], Gabriele Baniulyte[1†], Shivani S. Singh[1], Anne M. Stringer[2], Richard P. Bonocora[2], Mathew Stracy[3], Achillefs N. Kapanidis[3], Joseph T. Wade[2,4] and David C. Grainger[1*]

*for correspondence

Email: d.grainger@bham.ac.uk Tel: +44 (0)121 4145437

[1] Institute of Microbiology and Infection, School of Biosciences, University of Birmingham, Edgbaston, Birmingham, B15 2TT, UK

[2] Wadsworth Center, New York State Department of Health, Albany, NY, 12208, USA

[3] Biological Physics Research Group, Clarendon Laboratory, Department of Physics, University of Oxford, Oxford OX1 3PU, UK

[4] Department of Biomedical Sciences, School of Public Health, University at Albany, SUNY, Albany, NY, 12201, USA

[†] Present address: Department of Biomedical Sciences, School of Public Health, University at Albany, SUNY, Albany, NY, 12201, USA

ABSTRACT

Horizontal gene transfer permits rapid dissemination of genetic elements between individuals in bacterial populations. Transmitted DNA sequences may encode favourable traits. However, if acquired DNA has an atypical base composition, it can reduce host fitness. Consequently, bacteria have evolved strategies to minimise the harmful effects of foreign genes. Most notably, xenogeneic silencing proteins bind incoming DNA that has a higher AT-content than the host genome. An enduring question has been to understand why such sequences are deleterious. Here, we show that the toxicity of AT-rich DNA in *Escherichia coli* frequently results from constitutive transcription initiation within the coding regions of genes. Left unchecked, this causes titration of RNA polymerase and a global downshift in host gene expression. Accordingly, a mutation in RNA polymerase that diminishes the impact of AT-rich DNA on host fitness, reduces transcription from constitutive, but not activator-dependent, promoters.

INTRODUCTION

Bacteria obtain DNA from their environment by direct uptake (transformation), the action of viruses (transduction), or the acquisition of transmissible plasmids (conjugation)[1]. Thus, "horizontal" DNA transfer allows phenotypes to spread through bacterial populations. Transferred traits can be beneficial[1]. However, acquired sequences with a high AT-content may reduce host fitness[2-6]. Bacteria have developed mechanisms to diminish the toxicity of AT-rich genes. One approach involves a family of xenogeneic DNA binding proteins[7,8]. These proteins target DNA that has a higher AT-content than the host genome ("AT-rich" DNA), and silence transcription[9-12]. However, it is unclear why AT-rich DNA is toxic and why transcriptional silencing is beneficial.

The Histone-like Nucleoid Structuring (H-NS) protein of γ-proteobacteria is the best-characterised xenogeneic silencing protein[9,13]. To reduce transcription, H-NS oligomerises across AT-rich genes[9-12]. This process is triggered by nucleation at sequences containing a T:A step[14-19]. Intriguingly, promoter -10 hexamers (consensus 5'-TATAAT-3', recognised by the RNA polymerase σ^{70} subunit) are excellent inducers of H-NS nucleation[15,20]. Hence, H-NS can exclude RNA polymerase from, or trap RNA polymerase at, promoter DNA[8,9,21,22].

A challenge has been to understand why horizontally acquired AT-rich DNA is toxic. As we noted previously, such regions contain a disproportionally high number of promoter-like sequences[23-26]. Furthermore, we showed that H-NS suppresses transcription primarily from promoters that are intragenic and/or far from gene starts[25]. Here, we test the hypothesis that transcription from intragenic promoters is a major cause of toxicity in cells lacking H-NS. Working with a sub-set of AT-rich genes, we demonstrate dramatic effects of H-NS on intragenic transcription. When this transcription is disabled, associated fitness costs decrease. Genome-wide, if derepressed, intragenic transcription sequesters RNA polymerase. This causes a global downshift in canonical gene expression.

Accordingly, a mutation in RNA polymerase that reduces transcription from constitutive promoters, but not those that are activator-dependent, compensates for loss of H-NS.

RESULTS

Identification of the canonical yccE promoter

We chose *yccE* as a model gene to understand xenogeneic silencing. We selected *yccE* because it is AT-rich (66% A/T), silenced and bound by H-NS[27], and contains at least two intragenic promoters[25,28]. Importantly, *yccE* can be studied in isolation because the adjacent genes are not H-NS bound (Figure 1a). We sought to understand the source of *yccE* transcription in cells lacking H-NS. As a starting point, we identified the canonical *yccE* promoter. We were aided by previous observations that *yccE* is a target for σ^{32} (heat shock σ factor)[29]. Segments of the *yccE* intergenic region were fused to *lacZ* in reporter plasmid pRW50 (Figure S1a). Promoter activity located to a 55 base pair (bp) DNA fragment immediately upstream of *yccE* (Figure S1b). Figure 1b shows the sequence of this DNA fragment, named *yccE*Δ200. A σ^{32}-dependent promoter sequence is apparent. We monitored transcripts produced from this promoter (P*yccE*) *in vitro*. To do this, fragments from the *yccE* intergenic region were cloned upstream of the λ*oop* terminator in plasmid pSR. Transcripts initiating at P*yccE*, and terminating at λ*oop*, should be ~106 nucleotides (nt) in length. Coincidentally, the RNA-I transcript, derived from the pSR replication origin, is 108/107 nt long. To avoid confusing transcripts, we first monitored RNAs produced using pSR without a P*yccE* insert. The data show that σ^{32} dependent synthesis of the RNA-I transcript is inefficient (Figure 1c, compare lanes 1 and 2). When the entire *yccE* intergenic region was cloned in pSR σ^{32} dependent *yccE* transcripts were identified (Figure 1c, lane 3). The same transcripts were observed upon cloning the truncated *yccE*Δ200 fragment (Figure 1c, lane 4). A 10 bp truncation at the 5' end of *yccE*Δ200 abolished transcription (Figure 1c, lane 5). To confirm correct identification of P*yccE*, DNA recognition elements for σ^{32} were mutated (detailed in Figure 1b). All mutations greatly reduced promoter activity (Figure 1d).

Increased transcription of yccE *in Δ*hns *cells does not require P*yccE

Convention dictates that P*yccE* should cause increased *yccE* transcription in cells lacking H-NS. We considered this unlikely given the low activity, and σ^{32} dependence, of P*yccE*. Hence, we generated a series of *yccE::lacZ* fusions to investigate the contribution of P*yccE*. The different constructs, labelled *i* through *iv*, are illustrated below the graph in Figure 1e. We first measured *lacZ* expression in wild-type cells (Figure 1e, grey bars). When *yccE* was in the forward orientation, low-level *lacZ* expression was apparent. This was abolished upon deletion of P*yccE* (compare constructs *ii* and *iii*). In the reverse orientation, *yccE* stimulated higher *lacZ* expression (construct *iv*). This is consistent with our previous identification of a strong antisense promoter at the 5' end of *yccE* (adjacent to *lacZ* in this

assay)[28]. Remarkably, in the absence of H-NS, *lacZ* expression increased in all scenarios (Figure 1e, white bars). This transcription must be due to intragenic promoters.

The yccE *coding sequence is enriched for promoters*

A search identified 21 possible promoters within *yccE*. To test for function, we isolated promoters on 56 bp DNA fragments and fused them to *lacZ* (Figure 2a). Note that such sequences are too short to be subject to repression by H-NS[25,30]. Eleven DNA fragments stimulated β-galactosidase expression twofold or more above background (labelled A-K in Figure 2a). Under the conditions of our experiment, 7 of the 11 intragenic promoters were more efficient at driving transcription than P*yccE* (Figure 2a, black bar). Note that fragment "A" contains the strong antisense promoter described previously[28].

Transcription initiation within yccE *is repressed by H-NS* in vitro

In the context of the full *yccE* gene, intragenic promoters should be repressed by H-NS. We tested this *in vitro* using the pSR system. As noted above, with empty pSR, the 108/107 nt RNA-I transcript is produced. In addition, larger transcripts are generated from genes native to the plasmid. The complete set of transcripts produced from pSR is shown in Lane 1 of Figure 2b. In the figure, large (>1000 nt) pSR derived transcripts are highlighted by a black box and RNA-I is highlighted by a grey box. We introduced *yccE* into pSR, in either the forward or reverse orientation, upstream of the λ*oop* terminator. Since *yccE* is 1257 bp in length, most intragenic transcripts should be separable from pSR derived transcripts. As expected, numerous transcripts between 100 and 1000 nt in length were detected for both *yccE* containing plasmids (compare Lanes 1, 2 and 6 in Figure 2b). For the plasmid containing *yccE* in the reverse orientation an additional small transcript was detected (highlighted by lower blue box in Figure 2b). This was expected, the transcript generated from the strong antisense promoter at the 5' end of *yccE*, has a size of 90 nt in this assay. Regardless of *yccE* orientation, addition of H-NS inhibited synthesis of most *yccE* derived transcripts (Lanes 3-5 and 6-9). Synthesis of the RNA-I transcript was enhanced by H-NS suggesting that RNA polymerase is titrated by promoters within *yccE*.

Intragenic promoters are the source of increased yccE *transcription in cells lacking H-NS*

To confirm that H-NS repressed intragenic *yccE* promoters *in vivo*, we made derivatives of our *yccE*::*lacZ* fusions. The derivatives carry mutations in intragenic -10 elements. Schematics are below the graph in Figure 2c. The open arrows show *yccE* lacking internal promoters. Full details are in Figure S2. In the absence of H-NS, the ability of mutated *yccE* alleles to stimulate *lacZ* expression was reduced (Figure 2c). Thus, both biochemical and genetic inspection show silencing of intragenic transcription by H-NS. We refer to this as "pseudo-regulation" that occurs independently of, and may be mistaken for, the control of mRNA synthesis. Thus, supposed gene regulatory effects of H-NS may often be due to intragenic promoters.

The fitness cost of yccE is a consequence of intragenic transcription

We predicted a link between intragenic transcription and reduced fitness associated with loss of H-NS. Hence, *E. coli* M182, and the *hns*::kan variant, were transformed with pSR carrying *yccE* with or without internal promoters. Importantly, *yccE* mRNA cannot be expressed in this scenario; no upstream promoter is present. We monitored cultures inoculated with these strains (Figure 2d,e). In all cases, cells lacking *hns* had reduced fitness compared to the parent. However, this fitness defect was smaller for the *yccE* derivative lacking internal promoters (Figure 2e). Complete elimination of the fitness defect was not expected; AT-rich genes present on the *E. coli* chromosome also contribute.

Repression of intragenic transcription by H-NS reduces the fitness cost of many AT-rich genes

We identified other solitary genes targeted by H-NS: *yfdF*, *ykgH*, *yjgN* and *yjgL*. We cloned these, and derivatives lacking intragenic promoters, upstream of the λ*oop* terminator in pSR. The *fepE* gene, which has an AT-content of 55%, was included as a control. The constructs are illustrated above the gel image in Figure 3a. Full gene sequences are in Figure S3. Figure 3a shows results of *in vitro* transcription experiments. Whilst RNA polymerase did not initiate transcription within *fepE* (Lane 1), intragenic transcription was observed for *yfdF*, *ykgH*, *yjgN* and *yjgL* (Lanes 2, 4, 6 and 8). Mutation of intragenic promoters reduced this transcription (Lanes 3, 5, 7 and 9). The coding regions described above were also cloned upstream of *lacZ* in pRW50 (Figure 3b). Expression of *lacZ* was measured in M182 or the *hns*::kan derivative (Figure 3b). Upon deletion of *hns*, expression of *lacZ* downstream of *yfdF*, *ykgH*, *yjgN* or *yjgL*, but not *fepE*, increased (solid arrows). In contrast, no such increase occurred when intragenic promoters were mutated (open arrows). These analyses are consistent with silencing of intragenic promoters by H-NS at all loci tested. Hence, we measured the fitness cost of multicopy *yfdF*, *ykgH*, *yjgN* and *yjgL* in cells with and without H-NS. In all cases, the fitness deficit between wild-type and *hns*::kan cells decreased upon mutation of intragenic promoters (Figure 3c,d). Furthermore, changes in fitness and *lacZ* expression were significantly correlated (Figure S4a).

AT-rich genes titrate RNA polymerase and cause a global downshift in housekeeping transcription

RNA polymerase levels are limited in *E. coli*[31]. Consequently, multiple copies of a strong promoter can hinder growth and titrate transcription of the *lac* operon (Figure S4b). Interestingly, RNA polymerase levels do not increase in cells lacking H-NS (Figure S5). Therefore, competition for the enzyme must increase; more promoters compete for a limited supply of RNA polymerase. Logically, migration of RNA polymerase to spurious promoters should cause a global downshift in canonical transcription. However, despite many studies of the H-NS controlled transcriptome, a universal downshift has never been reported[9,10,27,32,33]. We reasoned that this might result from data normalisation approaches used previously. Briefly, transcriptome analysis compares RNA levels in two strains. Comparison requires a point of reference believed to be consistent between the strains. For example, it may be assumed that housekeeping genes are similarly transcribed or that averaged

transcription across all genes will be equivalent. Problematically, these approaches cannot differentiate between technical variation and genuine shifts in global transcription. To circumvent this problem, spiked-in RNA standards can be used[34]. We adapted this tactic to quantify global effects of H-NS on transcription. Briefly, we grew *E. coli* MG1655, and the *hns*::kan variant, to mid-log phase. We then counted colony-forming units for each *E. coli* culture. The same was done for a single culture of *Salmonella* Typhimurium. Accordingly, we were able to mix a defined number of clonal *S.* Typhimurium cells with each *E. coli* strain. The cell mixtures were subject to transcriptome analysis. For identically grown *S.* Typhimurium cells, differences in RNA abundance must result from processing variation. Hence, at the end of the procedure, transcripts mapping uniquely to *S.* Typhimurium were used to normalise the data. Figure 4a shows a post-normalisation plot of read depth for each *E. coli* gene in each strain. The diagonal blue line shows the expected position of data points if transcription is unchanged between strains. There is a downshift in transcription of genes not bound by H-NS (black). Conversely, H-NS bound genes (red) are transcribed more frequently. This behaviour is exemplified in Figure 4b.

RNA polymerase titration can be visualised directly

Genes bound by H-NS are overrepresented near the chromosome replication terminus (Ter)[35,36]. Conversely, most RNA polymerase binds near the origin of replication (Ori)[37]. These loci occupy distinct intracellular territories; Ter typically frequents mid-cell whilst Ori migrates to the poles[37-39]. Consequently, it should be possible to visualise titration of RNA polymerase at the cellular level. Previously, we used super resolution microscopy to track individual RNA polymerase molecules in live *E. coli*[40]. Here, we repeated this analysis to examine the effect of deleting *hns*. In wild-type cells, RNA polymerase clusters near the quarter cell positions (Figure 4c, top). However, in cells lacking H-NS, RNA polymerase is redistributed and mid-cell is occupied (Figure 4c, middle). Consistent with unaltered RNA polymerase abundance, occupancy of mid-cell corresponds to reduced RNA polymerase abundance elsewhere (Figure 4c).

RNA polymerase mutation can compensate for loss of H-NS by favouring regulated transcription

An aspartic acid substitution in the RNA polymerase σ^{70} subunit (G424D in *E. coli*) can compensate for loss of H-NS[41]. This side chain could clash with the promoter -10 element during transcription initiation[41]. According to our model, promoters within genes are constitutive; they rely solely on their DNA sequence to bind RNA polymerase. Conversely, canonical promoters are regulated; a complex array of transcriptional activators stabilise RNA polymerase binding and DNA unwinding[42]. We reasoned that transcriptional defects, due to the G424D mutation, might be more pronounced at constitutive promoters. To test this, we purified RNA polymerase containing σ^{70} or the G424D derivative. We then investigated the ability of the RNA polymerase derivatives to stimulate unwinding of a promoter -10 element using $KMnO_4$ footprinting. The semi-synthetic NM501

promoter was used because it has constitutive activity, by virtue of a consensus -10 element, but can be upregulated by the transcriptional activator CRP[43]. The G424D mutation completely abolished DNA opening by RNA polymerase in the absence of CRP (Figure 4d, compare lanes 2-5 and 6-9). In contrast, when CRP was present, the σ^{70} G424D mutation had little effect (compare lanes 10-13 and 14-17). Similarly, *in vivo*, the σ^{70} G424D mutation caused transcriptional defects at 7 of 8 constitutive promoters (Figure 4e). However, σ^{70} G424D functioned as well as, or better than, wild type RNA polymerase at activator dependent promoters (Figure 4f).

DISCUSSION

The AT-rich genes examined here impose a fitness cost due to intragenic promoters. This phenomenon is likely to be widespread in bacteria; functional homologues of H-NS are apparent in diverse species[8]. Furthermore, the DNA binding properties of RNA polymerase are highly conserved[42]. We suggest that misappropriation of cellular resources underlies the *hns* phenotype. Redeployment of the finite RNA polymerase pool causes uniform suppression of canonical transcription. Whilst this general effect is likely to be pervasive, we do not exclude organism-specific complications. For example, in *Pseudomonas aeruginosa*, loss of H-NS-like proteins causes prophage induction and cell death[44,45]. Interestingly, linear H-NS filaments do not pose a barrier to transit of RNA polymerase[46]. Accordingly, transcription of an mRNA, and silencing of intragenic promoters, could occur simultaneously. For example, in this work, P*yccE* was active both in isolation and upstream of H-NS bound *yccE*. We speculate that gene silencing by H-NS may have evolved to discriminate between canonical and spurious RNA synthesis.

MATERIALS AND METHODS

Strains, plasmids and general methods

E. coli JCB387 Δ*nir* Δ*lac* and MG1655 have been described previously[47,48]. M182*hns*::*kan* and KF26*hns*::*kan* were constructed by P1 transduction of *hns*::*kan* from MG1655 into the respective parent strains. The MG1655 *hns*::*kan* strain was provided by Ding Jin. M182*rpoD::kan* was generated using gene doctoring according to the protocol of Lee *et al*[49] using the plasmids and oligonucleotides listed in Table S1. Note that, prior to gene doctoring, M182 strains were transformed with plasmid pVRσ that encodes *rpoD*[50]. Quickchange mutagenesis was used to introduce the G424D mutation into pVRσ encoded *rpoD* (Table S1). Fortuitously, chromosomal and plasmid encoded σ^{70} were produced at indistinguishable levels (Figure S6). Sample sizes for all experiments were selected to ensure reproducibility in line with our previous work.

DNA fragments and gene expression assays

Promoter*::lacZ* fusions were made by cloning DNA fragments upstream of *lacZ* in the low copy number plasmid pRW50[51]. The nested deletions in the *yccE* intergenic region were generated by PCR

and oligonucleotides shown in Table S1. The various *yccE*, *yfdF*, *ykgH*, *yjgN* and *yjgL* alleles were synthesised by Invitrogen and some contain silent mutations to remove *Eco*RI or *Hin*dIII restriction sites to facilitate cloning (Figures S2a and S3). Oligonucleotides used to amplify the different alleles for cloning into pSR and pRW50 are shown in Table S1. The 56 bp intragenic *yccE* fragments were generated with overlapping oligonucleotides (Table S1). The resulting single stranded overhangs were filled with DNA polymerase before cloning. β-galactosidase assays were done using the protocol of Miller[52]. All assay values are the mean of three biological replicates and the error bars show standard deviation from the mean. Experiments were done at least twice. Cells were grown aerobically at 37°C, to mid-log phase, in LB media.

Bioinformatic analysis of genes and design of new coding regions

Our stringent search criteria selected putative σ^{70} dependent promoters as described previously[25]. Thus, sequences were selected that matched the motifs 5'-TAnAAT-3', 5'-TATnAT-3' or 5'-TATAnT-3'. The relaxed search selected the sequence 5'-TAnnnT-3'. To inactivate promoter -10 elements the initial 5'-TA-3' was replaced with 5'-GG-3'

Proteins, $KMnO_4$ footprinting and in vitro transcription assays

H-NS and RNA polymerase were prepared as described previously[53]. DNA fragments for $KMnO_4$ footprinting experiments were derived from Qiagen maxi-preparations of plasmid pSR. Thus, promoter DNA fragments were excised from pSR by sequential digestion with *Hin*dIII and then *Aat*II. After digestion fragments were labelled at the *Hin*dIII end using [γ-^{32}P]-ATP and polynucleotide kinase. Footprints were done as described by Grainger *et al*.[54]. The *in vitro* transcription experiments were done as described by Savery *et al*.[55] using the system of Kolb *et al*.[56]. A Qiagen maxiprep kit was used to purify supercoiled pSR plasmid carrying the different promoter inserts. This template (16 μg ml−1) was pre-incubated with purified H-NS in buffer containing 20 mM Tris pH 7.9, 5 mM MgCl2, 500 μM DTT, 50 mM KCl, 100 μg ml−1 BSA, 200 μM ATP, 200 μM GTP, 200 μM CTP, 10 μM UTP with 5 μCi [α-^{32}P]-UTP. The reaction was started by adding purified *E. coli* RNA polymerase. Labelled RNA products were analysed on a denaturing polyacrylamide gel. All *in vitro* assays were repeated at least three times in their entirety.

Growth assays

Cells lacking H-NS rapidly acquire compensatory mutations[41]. Consequently, reproducible changes in growth were only obtained when precautions were taken to minimise this phenomenon. The primary precaution was to reduce the number of division cycles that strains passed though during experimental setup. Thus, M182 and the *hns*::kan derivative were taken directly from long-term -80°C storage and used immediately to inoculate LB medium. After incubation for several hours at 37°C cells were harvested and competency was induced using ice cold $CaCl_2$. The cells were then transformed with desired plasmids and transformants were isolated on selective agar plates. A colony from each plate was suspended in LB medium and aliquots of this were used immediately to inoculate fresh media so

that growth could be monitored. Cells were grown either in LB medium at 37°C or in M9 minimal medium at 30°C. Values shown are from three biological replicates and the experiments were done on two separate occasions.

Western blotting

To determine relative protein levels in different strains cells were grown in LB media at 37°C. Aliquots of the culture were harvested at indicated time points and CFUs determined. Following this quantification the same number of cells from each aliquot were resuspended in SDS-PAGE gel loading buffer. After heating to 90°C for two minutes we separated proteins present in each lysate using SDS-PAGE. The proteins were then transfered to a Hybond-ECL nitrocellulose membrane using an Invitrogen XCell II Blot Module. Mouse anti-sera against the σ^{70} and β subunits of RNA polymerase (Neoclone) and H-NS (a gift from Jay Hinton) was used to detect the relevant proteins. Primary antibody binding was probed with horseradish peroxidise-linked rabbit anti-mouse antisera (Sigma-Aldrich A9044). The experiments were done on two separate occasions.

Standard RNA-seq

RNA-seq experiments were done in duplicate. *E. coli* MG1655 and *E. coli* MG1655 Δ*hns* were grown in LB medium at 30°C to an OD_{600} of 0.5-0.7. RNA was harvested, RNA-seq libraries were constructed and libraries were sequenced as described previously[57].

RNA-seq with a spiked in control

Transcriptome analysis experiments shown were performed in duplicate using *E. coli* MG1655 and *E. coli* MG1655 Δ*hns*. We also ran the same experiment, again in duplicate, using *E. coli* M182 and the *hns*::kan derivative. The results were near identical. For each replicate three mid-log phase bacterial cultures were prepared. The three cultures were *E. coli* MG1655, *E. coli* MG1655 Δ*hns* or *Salmonella* Typhimurium 14028s in LB medium. Before harvesting RNA the number of colony forming units (CFUs) per unit volume was determined for each culture by plating dilutions of each culture on nutrient agar and counting bacterial colonies. Aliquots of the two *E. coli* cultures were mixed *S.* Typhimurium cells. The volume of *Salmonella* cells was normalised to the CFUs for the corresponding *E. coli* culture. This step is crucial because it allows processing artefacts, due to differences in lysis efficiency, RNA recovery or cDNA synthesis, to be removed. Thus, in the final transcriptome analysis, the number of sequencing reads corresponding to the *S.* Typhimurium genome should be identical for each sample; they were derived from the same number of clonal *S.* Typhimurium cells. Hence, differences can only result from downstream processing. RNA was harvested, and RNA-seq libraries were prepared, as described previously[57]. RNA-seq libraries were sequenced on am Illumina Hi-Seq 2000 instrument (University at Buffalo, SUNY, Buffalo, NY, USA).

Data normalisation and transcriptome analysis

Our normalisation procedure is based on the addition of a proportional number of *S.* Typhimurium cells to each sample of *E. coli* cells immediately before harvesting RNA. All reads were first mapped to the *E. coli* MG1655 genome using CLC Genomics Workbench (Version 8.0; default parameters except that a perfect match was required). Unmapped reads were mapped to the *S.* Typhimurium 14028s genome (same parameters as above). The number of mapped *S.* Typhimurium reads, for each *E. coli* sample, was used to determine a correction factor for each sample. For example, if Sample A has twice as many *S.* Typhimurium reads as Sample B, the correction factor for Sample A will be twice that for Sample B. Having calculated a correction factor for each sample, we remapped all sequence reads to the *S.* Typhimurium 14028s genome using CLC Genomics Workbench (same parameters as above). Unmapped reads were then mapped to the *E. coli* MG1655 genome using CLC Genomics Workbench (same parameters as above). Total read coverage per gene was calculated using a custom Python script. These values were normalised to the length of the gene, and further normalised using the correction factor (described above). Raw data are available from the ArrayExpress database using accession number E-MTAB-4751.

Super resolution microscopy of RNA polymerase

Cell preparation, microscopy, and analysis were performed as described previously[40,58]. In brief, we used an endogenous fusion of photoactivatable fluorescent protein PAmCherry, with the β' subunit of RNA polymerase, encoded by *E. coli* strain KF26[58]. Glycerol stocks of KF26, and the *hns*::kan derivative, were used to inoculate fresh Rich Defined Media (RDM, Teknova). When the culture attained an OD_{650} value of ~0.2 cells were collected by centrifugation and resuspended. Cells in 1 µl of the suspension were placed on an RDM agarose pad and imaged for 300000 frames at 15 ms exposure on a custom built single-molecule TIRF microscope. For each strain, 9 fields of view were imaged. The experiment was done on 3 separate occasions. Molecules were imaged by photoactivating and localising fluorophores, and joining localisations over multiple frames to obtain trajectories of individual molecules. To measure RNA polymerase mobility, we calculated an apparent diffusion coefficient from the mean squared displacement of trajectories of individual molecules, and used a threshold to distinguish transcriptionally active and promoter bound molecules from the rest of the population. Cell outlines were determined from the brightfield image, and the average intracellular location of RNA polymerase was established from a 2D histogram of the mean trajectory positions relative to the cell outline for all DNA-bound molecules in at least 100 cells. Ter positioning was determined using similar analysis of strain PZ111 carrying a *tetO* array inserted at Ter, and expressing a TetR-mYpet fusion. The strain was constructed by P1 transduction of *tetR*-mYPet kan, into an AB1157 strain with an array of 240 *tetO* sequences 50 kb clockwise of *dif* (ter3)[59].

Data availability

The data that support these findings are available from the corresponding author upon request. The raw data for RNA-seq experiments are available from the ArrayExpress database using accession number E-MTAB-4751. Original gel images are shown in Figure S7.

ACKNOWLEDGEMENTS

This work was funded by Leverhulme Trust project grant (RPG-2013-147) and Wellcome Trust Career Development Fellowship (WT085092MA) awarded to D.C.G. Support for J.T.W. was a National Institutes of Health Director's New Innovator Award (1DP2OD007188). A.N.K. and M.S. were supported by BBSRC grant (BB/N018656/1; to ANK and MS), and a Wellcome Trust Investigatorship (110164/Z/15/Z; to ANK). We thank Jay Hinton for the gift of anti-H-NS anti-sera.

CONTRIBUTIONS

D.C.G. and J.T.W. designed the study and wrote the manuscript. L.E.L., G.B., S.S.S., A.M.S., R.P.B., and M.S. generated the data and prepared it for publication. M.S. and A.N.K. provided new analytical tools and critically discussed the manuscript with D.C.G. and J.T.W. All authors contributed to data analysis and interpretation.

REFERENCES

1. Soucy SM, Huang J, Gogarten JP. 2015. Horizontal gene transfer: building the web of life. *Nat Rev Genet* **16:** 472-482.

2. Doyle M, Fookes M, Ivens A, Mangan MW, Wain J, Dorman CJ. 2007. An H-NS-like stealth protein aids horizontal DNA transmission in bacteria. *Science* **315:** 251-252.

3. Popa O, Hazkani-Covo E, Landan G, Martin W, Dagan T. 2011. Directed networks reveal genomic barriers and DNA repair bypasses to lateral gene transfer among prokaryotes. *Genome Res* **21:** 599-609.

4. Popa O, Dagan T. 2011. Trends and barriers to lateral gene transfer in prokaryotes. *Curr Opin Microbiol* **145:** 615-623

5. Raghavan R, Kelkar YD, Ochman H. 2012. A selective force favoring increased G+C content in bacterial genes. *Proc Natl Acad Sci* **109:** 14504-14507.

6. Baltrus DA. 2013. Exploring the costs of horizontal gene transfer. *Trends Ecol Evol* **8:** 489-495.

7. Dorman CJ. 2007. H-NS, the genome sentinel. *Nat Rev Microbiol*. **5:** 157-61.

8. Singh K, Milstein JN, Navarre WW. 2016. Xenogeneic Silencing and Its Impact on Bacterial Genomes. *Annu Rev Microbiol*. **70:** 199-213.

9. Navarre WW, Porwollik S, Wang Y, McClelland M, Rosen H, Libby SJ, Fang FC. 2006. Selective silencing of foreign DNA with low GC content by the H-NS protein in Salmonella. *Science* **313:** 236-238.

10. Lucchini S, Rowley G, Goldberg MD, Hurd D, Harrison M, Hinton JC. 2006. H-NS mediates the silencing of laterally acquired genes in bacteria. *PLoS Pathog* **28:** e81.

11. Smits WK, Grossman AD. 2010. The transcriptional regulator Rok binds A+T-rich DNA and is involved in repression of a mobile genetic element in Bacillus subtilis. *PLoS Genet* **6:** e1001207

12. Gordon BR, Li Y, Wang L, Sintsova A, van Bakel H, Tian S, Navarre WW, Xia B, Liu J. 2010. Lsr2 is a nucleoid-associated protein that targets AT-rich sequences and virulence genes in Mycobacterium tuberculosis. *Proc Natl Acad Sci* **107:** 5154-5159.

13. Dorman CJ. 2014. H-NS-like nucleoid-associated proteins, mobile genetic elements and horizontal gene transfer in bacteria. *Plasmid* **75:** 1-11.

14. Bouffartigues E, Buckle M, Badaut C, Travers A, Rimsky S. 2007. H-NS cooperative binding to high-affinity sites in a regulatory element results in transcriptional silencing. *Nat Struct Mol Biol* **14:** 441-418.

15. Gordon BR, Li Y, Cote A, Weirauch MT, Ding P, Hughes TR, Navarre WW, Xia B, Liu J. 2011. Structural basis for recognition of AT-rich DNA by unrelated xenogeneic silencing proteins. *Proc Natl Acad Sci* **108:** 10690-10695.

16. Arold ST, Leonard PG, Parkinson GN, Ladbury JE. 2010. H-NS forms a superhelical protein scaffold for DNA condensation. *Proc Natl Acad Sci* **107:** 15728-15732.

17. Amit R, Oppenheim AB, Stavans J. 2003. Increased bending rigidity of single DNA molecules by H-NS, a temperature and osmolarity sensor. *Biophys J* **84:** 2467-73.

18. Dame RT, Noom MC, Wuite GJ. 2006. Bacterial chromatin organization by H-NS protein unravelled using dual DNA manipulation. *Nature*. **444:** 387-390.

19. Liu Y, Chen H, Kenney LJ, Yan J. 2010. A divalent switch drives H-NS/DNA-binding conformations between stiffening and bridging modes. *Genes Dev*. **24:**339-44.

20. Landick R, Wade JT, Grainger DC. 2015. H-NS and RNA polymerase: a love-hate relationship? *Curr Opin Microbiol* **24:** 53-59.

21. Winardhi RS, Yan J, Kenney LJ. 2015. H-NS Regulates Gene Expression and Compacts the Nucleoid: Insights from Single-Molecule Experiments. *Biophys J*. **109:** 1321-1329.

22. Dame RT, Wyman C, Wurm R, Wagner R, Goosen N. 2002. *J Biol Chem* **277:** 2146-2150.

23. Huang Q, Cheng X, Cheung MK, Kiselev SS, Ozoline ON, Kwan HS. 2012. High-density transcriptional initiation signals underline genomic islands in bacteria. *PLoS One* **7:** e33759.

24. Singh SS and Grainger DC. 2013. H-NS can facilitate specific DNA-binding by RNA polymerase in AT-rich gene regulatory regions. *PLoS Genet* **9:** e1003589.

25. Singh SS, Singh N, Bonocora RP, Fitzgerald DM, Wade JT, Grainger DC. 2014. Widespread suppression of intragenic transcription initiation by H NS *Genes Dev* **28:** 214-219.

26. Lam KN and Charles TC. 2015. Strong spurious transcription likely contributes to DNA insert bias in typical metagenomic clone libraries. *Microbiome* **3:** 22.

27. Kahramanoglou C, Seshasayee AS, Prieto AI, Ibberson D, Schmidt S, Zimmermann J, Benes V, Fraser GM, Luscombe NM. 2011. Direct and indirect effects of H-NS and Fis on global gene expression control in *Escherichia coli*. *Nucleic Acids Res* **39:** 2073-91.

28. Chintakayala K, Singh SS, Rossiter AE, Shahapure R, Dame RT, Grainger DC. 2013. *E. coli* Fis protein insulates the *cbpA* gene from uncontrolled transcription. *PLoS Genet* **9:** e1003152.

29. Wade JT, Castro Roa D, Grainger DC, Hurd D, Busby SJ, Struhl K, Nudler E. 2006. Extensive functional overlap between sigma factors in *Escherichia coli*. *Nat Struct Mol Biol*. **13:** 806-814.

30. Haycocks JR, Sharma P, Stringer AM, Wade JT, Grainger DC. 2015. The molecular basis for control of ETEC enterotoxin expression in response to environment and host. *PLoS Pathog* **11:**e1004605.

31. Piper SE, Mitchell JE, Lee DJ, Busby SJ. 2009. A global view of *Escherichia coli* Rsd protein and its interactions. *Mol Biosyst* **5:** 1943-1947.

32. Srinivasan R, Scolari VF, Lagomarsino MC, Seshasayee AS. 2015. The genome-scale interplay amongst xenogene silencing, stress response and chromosome architecture in *Escherichia coli*. *Nucleic Acids Res*. **43:** 295-308.

33. Oshima T, Ishikawa S, Kurokawa K, Aiba H, Ogasawara N. 2006. *Escherichia coli* histone-like protein H-NS preferentially binds to horizontally acquired DNA in association with RNA polymerase. *DNA Res* **13:** 141-53.

34. Lovén J, Orlando DA, Sigova AA, Lin CY, Rahl PB, Burge CB, Levens DL, Lee TI, Young RA. 2012. Revisiting global gene expression analysis. *Cell* **151:** 476-482.

35. Lawrence JG, Ochman H. 1998. Molecular archaeology of the *Escherichia coli* genome. *Proc. Natl. Acad. Sci.* USA. **95:** 9413-9417.

36. Zarei M, Sclavi B, Cosentino Lagomarsino M. 2013. Gene silencing and large-scale domain structure of the *E. coli* genome. *Mol Biosyst*. **9:** 758-767.

37. Dame RT, Kalmykowa OJ, Grainger DC. 2011. Chromosomal macrodomains and associated proteins: implications for DNA organization and replication in Gram negative bacteria. *PLoS Genet*. **7:** e1002123.

38. Junier I, Boccard F, Espéli O. 2014. Polymer modeling of the *E. coli* genome reveals the involvement of locus positioning and macrodomain structuring for the control of chromosome conformation and segregation. *Nucleic Acids Res*. **42:** 1461-1473.

39. Youngren B, Nielsen HJ, Jun S, Austin S. 2014. The multifork *Escherichia coli* chromosome is a self-duplicating and self-segregating thermodynamic ring polymer. *Genes Dev*. **28:** 71-84.

40. Stracy M, Lesterlin C, Garza de Leon F, Uphoff S, Zawadzki P, Kapanidis AN. 2015. Live-cell superresolution microscopy reveals the organization of RNA polymerase in the bacterial nucleoid. *Proc Natl Acad Sci* USA. **112:** E4390-9.

41. Ali SS, Soo J, Rao C, Leung AS, Ngai DH, Ensminger AW, Navarre WW. 2014. Silencing by H-NS potentiated the evolution of *Salmonella*. *PLoS Pathog* **10:** e1004500.

42. Lee DJ, Minchin SD, Busby SJ. 2012. Activating transcription in bacteria. *Annu Rev Microbiol*. **66:** 125-152.

43. Miroslavova NS and Busby SJ. 2006. Investigations of the modular structure of bacterial promoters. *Biochem Soc Symp* **73:** 1-10.

44. Castang S, McManus HR, Turner, KH, Dove, SL. 2008. H-NS family members function coordinately in an opportunistic pathogen. *Proc. Natl. Acad. Sci*. USA **105:** 18947-18952.

45. Li C, Wally H, Miller SJ, Lu CD. 2009. The Multifaceted Proteins MvaT and MvaU, Members of the H-NS Family, Control Arginine Metabolism, Pyocyanin Synthesis, and Prophage Activation in *Pseudomonas aeruginosa* PAO1. *J. Bacteriol*. **191:** 6211-6218.

46. Kotlajich MV, Hron DR, Boudreau BA, Sun Z, Lyubchenko YL, Landick R. 2015. Bridged filaments of histone-like nucleoid structuring protein pause RNA polymerase and aid termination in bacteria. *Elife* **4:** e04970.

47. Page L, Griffiths L, Cole JA. 1990. Different physiological roles of two independent pathways for nitrite reduction to ammonia by enteric bacteria. *Arch Microbiol* **154:** 349-354.

48. Keseler IM, Mackie A, Peralta-Gil M, Santos-Zavaleta A, Gama-Castro S, Bonavides-Martínez C, Fulcher C, Huerta AM, Kothari A, Krummenacker M, *et al*. 2013. EcoCyc: fusing model organism databases with systems biology. *Nucleic Acids Res* **41:** D605-12.

49. Lee, DJ, Bingle LE, Heurlier K, Pallen MJ, Penn CW, Busby SJ, Hobman JL. 2009. Gene doctoring: a method for recombineering in laboratory and pathogenic *Escherichia coli* strains. *BMC Microbiol* **9:** 252.

50. Rhodius VA, Busby SJ. 2000. Interactions between activating region 3 of the *Escherichia coli* cyclic AMP receptor protein and region 4 of the RNA polymerase sigma70 subunit: application of suppression genetics. *J Mol Biol* **299:** 311-324.

51. Lodge J, Fear J, Busby S, Gunasekaran P, Kamini NR. 1992. Broad host range plasmids carrying the *Escherichia coli* lactose and galactose operons. *FEMS Microbiol Lett*. **74:** 271-276.

52. Miller J 1972. Experiments in Molecular Genetics. Cold Spring Harbor, NY: Cold Spring Harbor Laboratory Press.

53. Grainger DC, Goldberg MD, Lee DJ, Busby SJ. 2008. Selective repression by Fis and H-NS at the *Escherichia coli dps* promoter. *Mol Microbiol* **68:** 1366-1377.

54. Grainger DC, Belyaeva TA, Lee DJ, Hyde EI, Busby SJ. 2004. Transcription activation at the *Escherichia coli melAB* promoter: interactions of MelR with the C-terminal domain of the RNA polymerase alpha subunit. *Mol Microbiol* **51:** 1311-1320.

55. Savery NJ, Lloyd GS, Kainz M, Gaal T, Ross W, Ebright RH, Gourse RL, Busby SJ. *et al*. 1998. Transcription activation at Class II CRP-dependent promoters: identification of determinants in the C-terminal domain of the RNA polymerase alpha subunit. *EMBO J* **17:** 3439-3447.

56. Kolb A, Kotlarz D, Kusano S, Ishihama A 1995. Selectivity of the *Escherichia coli* RNA polymerase E sigma 38 for overlapping promoters and ability to support CRP activation. *Nucleic Acids Res* **23:** 819-826.

57. Stringer AM, Currenti S, Bonocora RP, Baranowski C, Petrone BL, Palumbo MJ, Reilly AA, Zhang Z, Erill I, Wade JT. 2014. Genome-scale analyses of *Escherichia coli* and Salmonella enterica AraC reveal noncanonical targets and an expanded core regulon. *J Bacteriol* **196:** 660-671.

58. Endesfelder U, Finan K, Holden SJ, Cook PR, Kapanidis AN, Heilemann M. 2013. Multiscale spatial organization of RNA polymerase in *Escherichia coli*. *Biophys J*. **105:** 172-181.

59. Zawadzki P, Stracy M, Ginda K, Zawadzka K, Lesterlin C, Kapanidis AN, Sherratt DJ. 2015. The Localization and Action of Topoisomerase IV in *Escherichia coli* Chromosome Segregation Is Coordinated by the SMC Complex, MukBEF. *Cell Rep*. **13:** 2587-2596.

FIGURES

Figure 1: Characterisation of the *yccE* locus.
a) Genomic context of *yccE* and its promoter. The panel shows *yccE*, and surrounding genes, alongside data describing H-NS binding (ChIP-seq[27]) and RNA abundance (standard RNA-seq; this work, done in duplicate). Data are representative.
b) Sequence of the *yccE*Δ200 DNA fragment containing P*yccE*. The P*yccE* -10 and -35 elements are in bold and underlined. A consensus σ^{32} promoter sequence is in grey for comparison. Mutations made to disrupt sequence elements are in red. Transcription can initiate at adjacent nucleotides. These are labelled (+1) and are highlighted by a bent arrow.
c) Analysis of transcripts generated from P*yccE* *in vitro*. The gel image shows transcripts generated by RNA polymerase, associated with either σ^{70} or σ^{32}, from pSR plasmid DNA templates. The schematic diagrams above the gel image represent the native cloning site of pSR (left hand side) or derivatives containing a P*yccE* insert (right hand side). The different P*yccE* containing DNA fragments inserted are indicated below the gel image in parenthesis. P*yccE* derived transcripts manifest as a 107/106 nucleotide (nt) doublet. The 108/107 nt RNA-I transcript is derived from the plasmid replication origin. The experiment was done three times. Data are representative.
d) Effect of P*yccE* mutation *in vivo*. The graph shows LacZ activity data obtained from *E. coli* JCB387 cells carrying different *yccE*Δ200 derivatives cloned in pRW50. Assays were done in triplicate and error bars show standard deviation from the mean.
e) Induction of *yccE* transcription in the absence of H-NS does not require P*yccE* *in vivo*. The panel illustrates a series of *yccE*::*lacZ* fusions labelled *i*-*iv*. Genes are shown as block arrows and P*yccE* is shown as a bent line arrow. The β-galactosidase activity was measured in lysates of M182 (grey bars) and M182*hns*::kan cells (open bars). Assays were done in triplicate and error bars show standard deviation from the mean.

Figure 2: H-NS represses intragenic *yccE* transcription and associated fitness costs
a) Identification of intragenic *yccE* promoters. The data are β-galactosidase activities driven by short intragenic *yccE* DNA fragments in strain JCB387. The bars align with the location of the DNA fragment relative to *yccE* and show sense (upper) and antisense (lower) transcription. Bars labelled "a"-"k" have at least 2-fold over background activity (empty pRW50; shown by dashed line). The black bar represents the canonical promoter P*yccE*. Note that, two DNA fragments resisted cloning. Hence, 19 of the 21 potential promoters were tested. Assays were done in triplicate. Error bars show standard deviation from the mean.
b) Transcription can initiate at multiple sites within *yccE* *in vitro*. Gel image showing RNA generated *in vitro* separated by denaturing gel electrophoresis. DNA templates, with the *yccE* gene cloned upstream of the λ*oop* terminator in plasmid pSR, are illustrated above the gel. Transcripts generated by RNA polymerase (400 nM) with empty pSR plasmid (lane 1) are highlighted by a black dashed line. Transcripts initiating within *yccE* in the forward (lanes 2-5) or reverse (lanes 6-9) orientation are highlighted by a blue dashed line. The control RNA-I transcripts are highlighted by a grey dashed line. H-NS was added at concentrations of 0.8, 1.5, or 3.0 μM. The experiment, done three times, is representative.

c) Mutation of promoters within *yccE* prevents induction in Δ*hns* cells. The lower illustrations show *yccE* (blue arrows) cloned upstream of *lacZ* (red arrow). A solid blue arrow represents wild type *yccE* whereas open arrows indicate *yccE* with mutated intragenic promoter -10 elements. For each *lacZ* fusion, β-galactosidase activity was measured in lysates of M182 (grey bars) and M182*hns*::kan cells (open bars). Assays were done in triplicate and error bars show standard deviation from the mean.

d,e) The fitness cost of *yccE* is reduced when intragenic promoters are mutated. The figure illustrates changes in culture OD_{650} following inoculation of LB medium. The inoculum was M182 (solid line) or M182*hns*::kan (dashed line) transformed with the pSR plasmid carrying d) wild type *yccE* or e) *yccE* with internal promoter -10 elements mutated. Cells were grown at 37°C. The experiment was done in triplicate. Error bars show standard deviation from the mean.

Figure 3: H-NS represses intragenic transcription and associated fitness costs at many loci.

a) Transcription initiation within the coding regions of H-NS target genes *in vitro*. An *in vitro* transcription assay using different AT-rich genes, cloned upstream of the λ*oop* terminator in plasmid pSR, as a template. The different DNA constructs are illustrated above the gel. The cloned genes have an AT-content of 65% (*yfdF*), 63% (*ykgH*), 63% (*yjgN*) and 68% (*yjgL*). For each cloned gene a solid arrow represents the wild type DNA sequence whereas an open arrow is a derivative where intragenic promoter -10 elements have point mutations. Note that the *fepA* gene was used as a control and has an AT-content of 55%. The positions of transcripts generated by RNA polymerase (400 nM) from the *fepE* control (lane 1) or the other cloned genes (lanes 2-9) are labelled. The *in vitro* transcription assays were run on three separate occasions. Data are representative.

b) Increased transcription in cells lacking H-NS frequently requires intragenic promoters *in vivo*. The panel illustrates a series of DNA constructs where different gene coding regions have been cloned upstream of *lacZ* (red arrow). For each cloned gene a solid arrow represents the wild type DNA sequence whereas an open arrow is a derivative where intragenic promoter -10 elements have point mutations. The cloned genes have an AT-content of 65% (*yfdF*), 63% (*ykgH*), 63% (*yjgN*) and 68% (*yjgL*). Note that the *fepA* gene is used as a control and has an AT-content of 55%. For each *lacZ* fusion β-galactosidase activity was measured in lysates of M182 (grey bars) and M182Δ*hns* (open bars) cells. Assays were done in triplicate and error bars show standard deviation from the mean.

c,d) The toxicity of many AT-rich genes is a consequence of spurious intragenic transcription. The figure illustrates growth of M182 (solid line) or M182*hns*::kan (dashed line) cells transformed with the pSR plasmid carrying different AT-rich genes. Panel c) shows wild type gene derivatives and d) shows derivatives with internal promoter -10 elements mutated (open arrows). Experiments were done using M9 minimal media at 30°C. The experiment was done in triplicate and error bars show standard deviation from the mean.

Figure 4: Most transcription is uniformly downregulated in cells lacking H-NS.

a,b) Most transcription is uniformly downregulated in cells lacking H-NS. a) the plot illustrates changes in global transcription caused by loss of H-NS. Data points represent H-NS bound (red) and unbound (black) genes. Genes with unaltered transcription should fall on the diagonal blue line. Data are from duplicate RNA-seq experiments. b) The basally expressed *fad* genes whose transcription is reduced in the absence of H-NS. Genes bound by H-NS are in red and other genes are black. Graphs show H-NS binding[27] and RNA abundance (RNA-seq with spiked in control; this work). Data are representative.

c) RNA polymerase is redistributed in cells lacking H-NS. RNA polymerase distribution in wild type (top) and *hns*::kan cells (middle). Each heat map shows the average position of DNA-bound (i.e. transcribing or interacting with a promoter) RNA polymerase molecules within the cell. The bottom panelshows the average position of Ter as determined by visualising a TetR-mYpet fusion bound at an array of Ter proximal *tetO* sequences. Each distribution was generated from 100 cells between 3.5 and 4.5 μm in length. Each square is 1/624 of total cell area.

d) The σ^{70} G424D mutation hinders constitutive but not activator dependent NM501 promoter activity *in vitro*. $KMnO_4$ footprinting reactions analysed on a denaturing polyacrylamide gel. Bands are indicative of open complex near the transcription start site (+1). RNA polymerase added at

concentrations of 200, 250, 300 or 350 nM and CRP was 1.0 μM. The experiment, done three times, is representative.

e,f) The σ^{70} G424D mutation hinders constitutive but not activator dependent promoter activity *in vivo*. Different promoter DNA fragments were cloned upstream of *lacZ* (red arrow). For each promoter the location of key DNA sequence elements is represented by a box. In each case, the box is coloured according to the relationship between the DNA sequence and the consensus sequence for that element: perfect (dark blue), imperfect (pale blue) or completely absent (white). For each *lacZ* fusion β-galactosidase activity was measured in lysates of JCB387*rpoD*::kan carrying pVRσ (white bars) or pVRσ^{G424D} (black bars). The experiment was done in triplicate. Error bars show standard deviation from the mean.

Lamberte_Figure 1

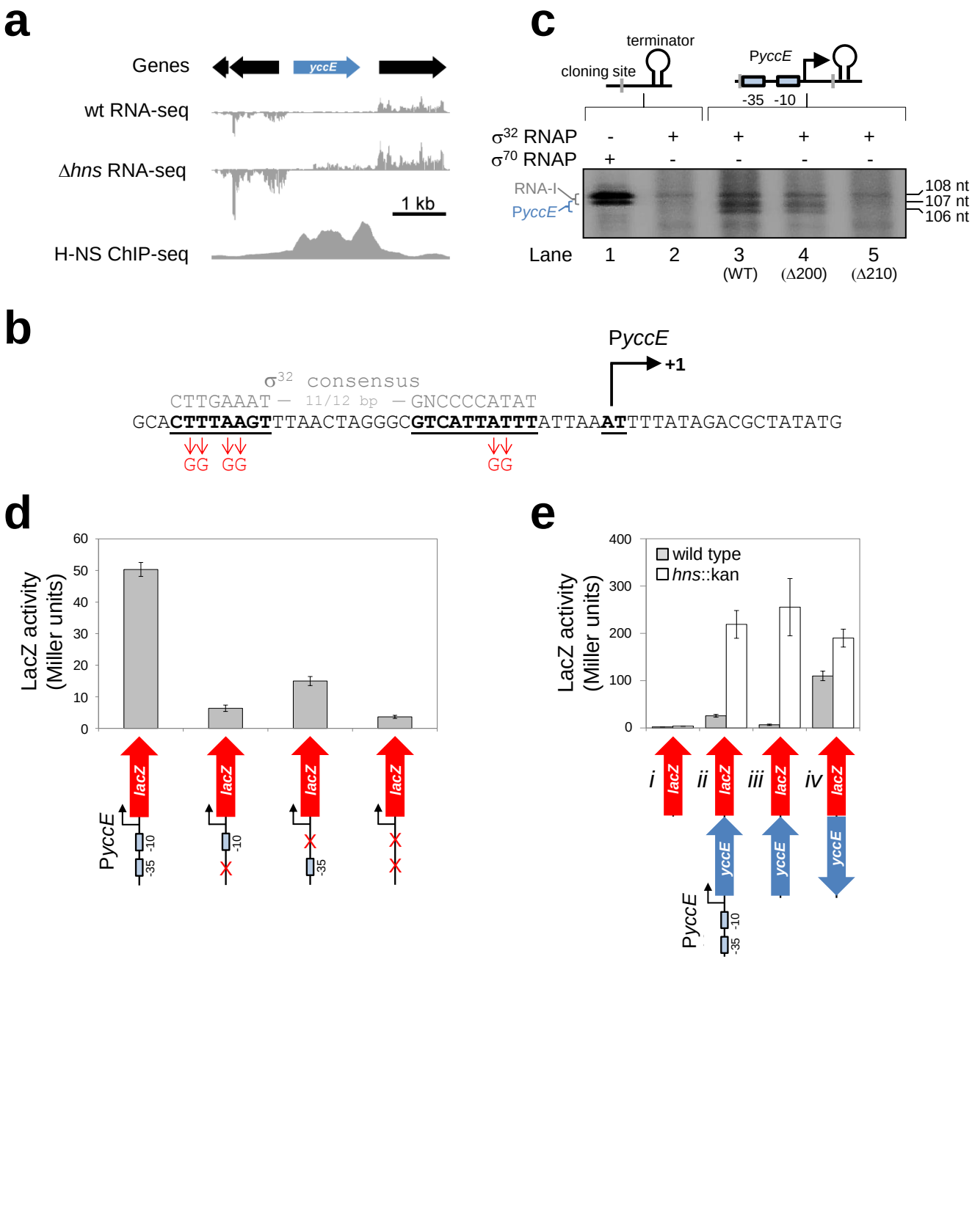

Lamberte_Figure 2

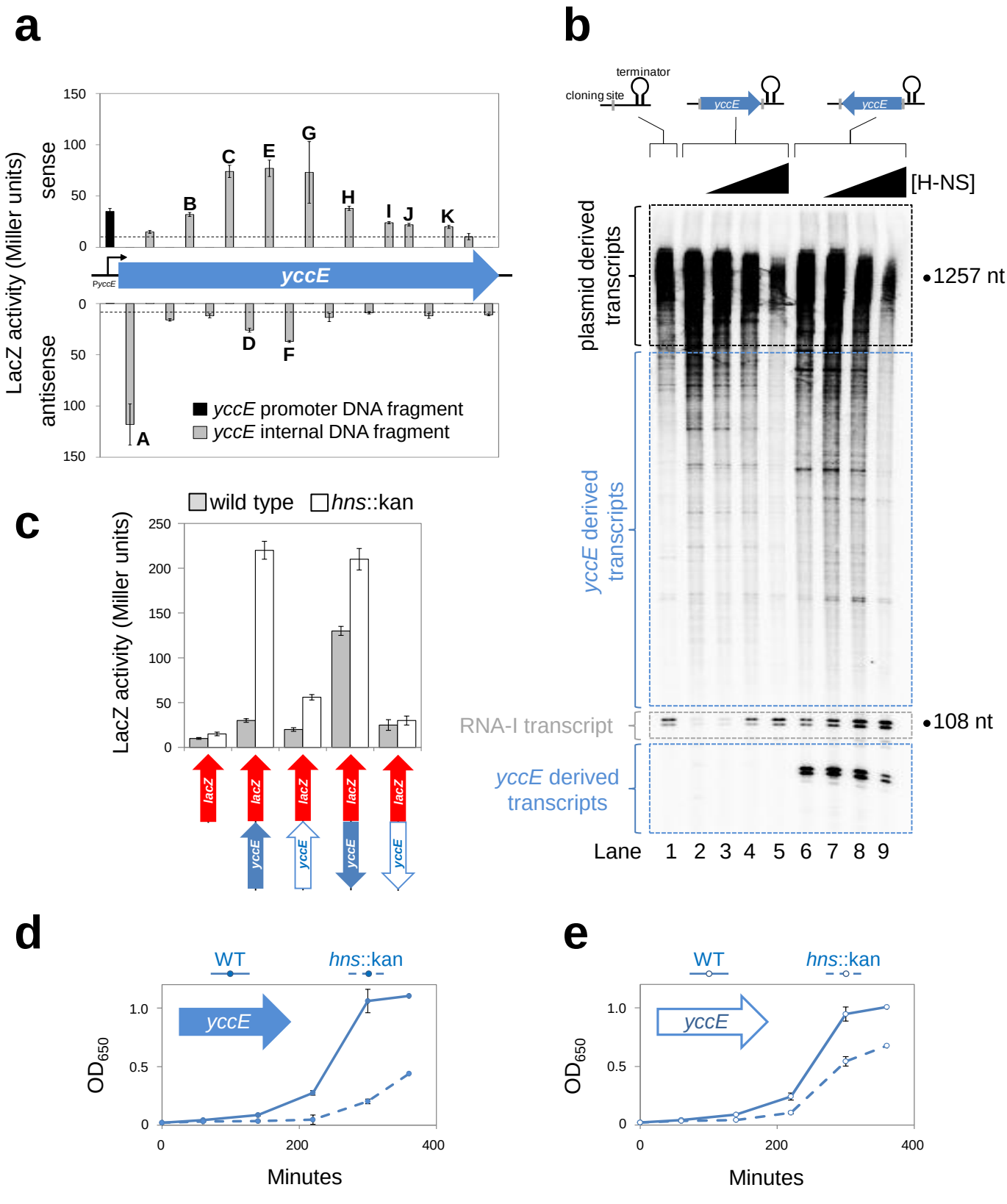

Lamberte_Figure 3

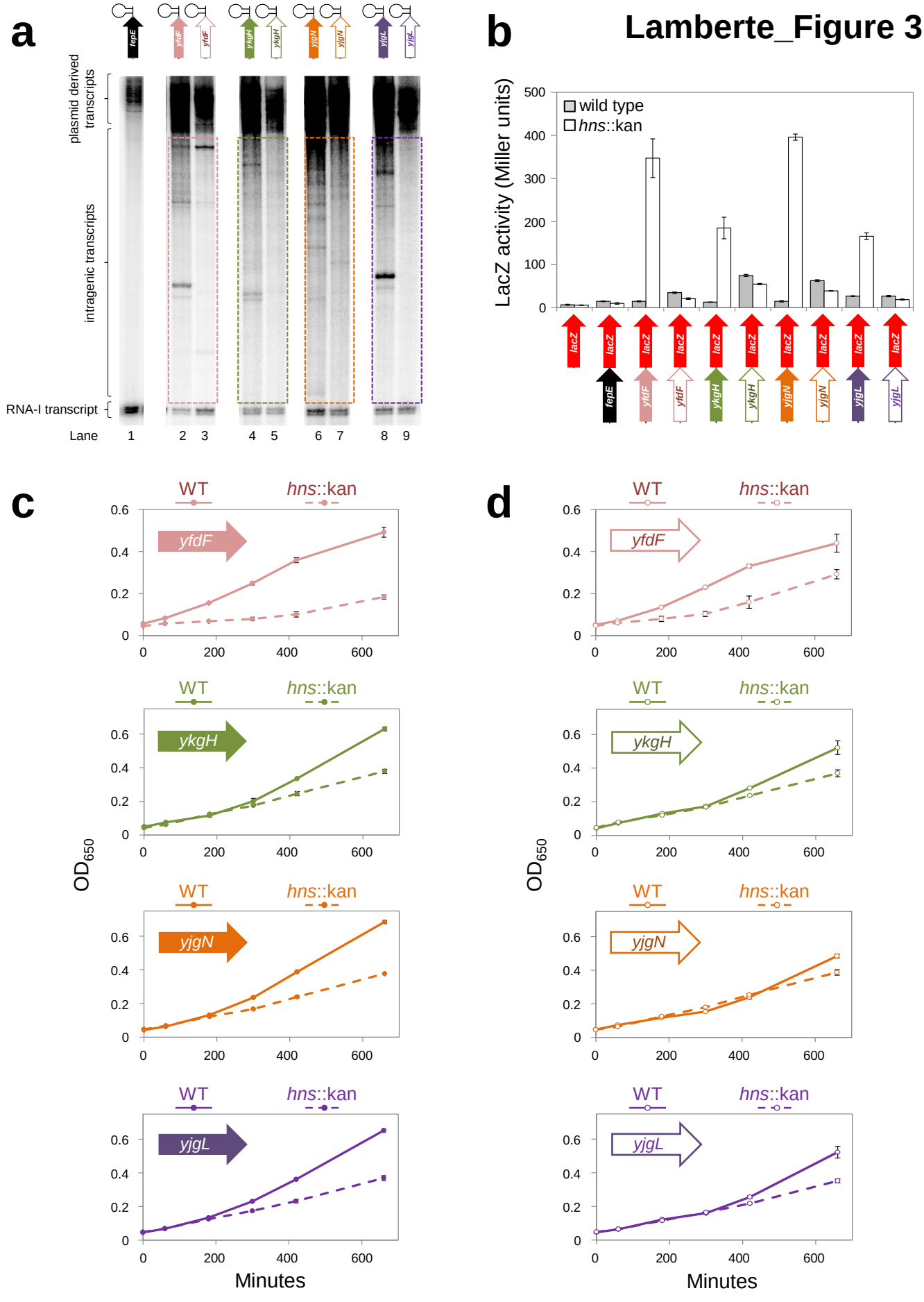

Lamberte_Figure 4